High-Speed Multipass Coulter Counter with Ultrahigh Resolution

Martin A. Edwards,[†] Sean R. German,[†,‡] Jeffrey E. Dick,[§] Allen J. Bard,[§] and Henry S. White*,[†]

[†]Department of Chemistry, University of Utah, Salt Lake City, Utah 84112, United States, [‡]Revalesio Corporation, 1200 East D Street, Tacoma, Washington 98421, United States, and [§]Center for Electrochemistry, Department of Chemistry, The University of Texas at Austin, Austin, Texas 78712, United States

ABSTRACT Coulter counters measure the size of particles in solution by passing them through an orifice and measuring a resistive pulse, *i.e.*, a drop in the ionic current flowing between two electrodes placed on either side of the orifice. The magnitude of the pulse gives information on the size of the particle; however, resolution is limited by variability in the path of the translocation, due to the Brownian motion of the particle. We present a simple yet powerful modified Coulter counter that uses programmable data acquisition hardware to switch the voltage after sensing the resistive pulse of a nanoparticle passing through the orifice of a nanopipet. Switching the voltage reverses the direction of the driving force on the particle and, when this detect—switch cycle is repeated, allows us to pass an individual nanoparticle through the orifice thousands of times. By measuring individual particles more than 100 times per second we rapidly determine the distribution of the resistive pulses for each particle, which allows us to accurately determine the mean pulse amplitude and deliver considerably improved size resolution over a conventional Coulter counter. We show that single polystyrene nanoparticles can be shuttled back and forth and monitored for minutes, leading to a precisely determined mean blocking current equating to sub-angstrom size resolution.
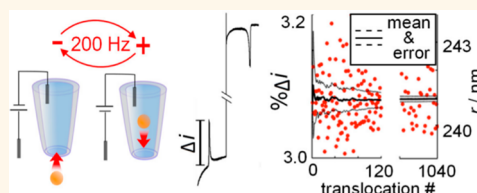
KEYWORDS: nanopore · nanopipet · Coulter method · resistive-pulse analysis · particle sizing · nanoparticles

Nanoparticles[1] are used in a diverse range of applications, *e.g.*, for electrocatalysis,[2,3] as MRI contrast agents,[4,5] and as quantum dots.[6] Nanoparticle-like structures are also found in biology, such as viruses,[7] vesicles,[8,9] and biomacromolecules.[10] Many properties of nanoparticles are highly size-dependent;[1,3,5] thus accurate determination of their size is important for their applications. The methods for generating nanoparticles typically result in a distribution of differently sized particles, and even so-called "monodisperse" nanoparticles show some degree of size variation (*e.g.*, <10%[11]); hence a measurement that gives the size distribution is desired.

Dynamic light scattering[12] (DLS) is commonly used to calculate the particle size distribution in solution. It is underpinned by the inverse problem of deriving the size distribution from scattering correlation data, which is ill-posed, meaning assumptions on the form of the particle size distribution are necessary to fit the data.[13] Analysis of electron microscopy images provides a direct measure of the size of individual nanoparticles;[14,15] however, preparing samples can introduce artifacts,[16] especially for soft structures,[17] and instrumentation is expensive. Nanoparticle tracking analysis[18] infers the size of individual particles by tracking the random-walk movement of the nanoparticles and attaining a diffusion coefficient, which is then used to calculate the hydrodynamic radius of the nanoparticle using the Stokes—Einstein relationship. The optical instrumentation, however, is expensive, and the technique assumes that all analytes are spherical. Moreover, the accuracy of the measurement relies on particles remaining in the field of view for sufficient time to develop accurate estimation of the diffusion coefficient.

Coulter counters measure the size of particles in solution by passing them through an orifice and measuring a resistive pulse, *i.e.*, a drop in the ionic current flowing between two electrodes placed on either side of the orifice.[19] These sensors have been used to characterize particles from the micrometer to the molecular scale, providing information about size and concentration,[20−24] surface charge,[21,25,26] shape,[27−30] deformability,[31,32] and conductivity.[33] The magnitude of the pulse is proportional to the particle's volume and should therefore be exquisitely sensitive

for sizing purposes. However, the technique's resolution has been limited by the short duration of the pulse and variability in the exact path of the translocation, due to Brownian motion of the particle.

Previously we demonstrated that the net force on a nanoparticle within a conical nanopore, which arises from the combination of electroosmotic flow, pressure driven flow, and electrophoresis, can be tuned to alter the direction of travel of a nanoparticle.[34] Recently we combined this concept with resistive pulse sensing to create an instrument that is able to perform multiple resistive pulse measurements of a single particle.[35] Upon detecting a resistive pulse indicating the passage of a particle through the pore orifice, a computer-controlled pressure controller reversed the net force on the particle; this drove the particle back through the pore, where it was again detected and the force (pressure) reversed. Repeating the detection−switching cycle effectively "traps" the particle to a region close to the pore aperture. We demonstrated trapping of nanoparticles performing many 10's of resistive pulse measurements on an individual nanoparticle and determining the mean resistive pulse magnitude with much higher resolution than possible with a traditional Coulter counter. A similar device using a cylindrical pore ∼30/70 μm in diameter was reported by Berge and co-workers.[27,36] Our nanopore-based system had some drawbacks; the control-loop that sensed and switched the pressure had a relatively slow response time, and typically ∼10 measurements per second could be made. The response time directly affects the number of measurements that can be recorded in a given time. Indirectly it affects the stability of trapping; the random walking of a particle means that it may wander out of the sphere of influence of the applied force before the direction of the force is reversed.

In this work we present a multipass Coulter counter, illustrated schematically in Figure 1, which uses programmable data acquisition hardware to switch the voltage after sensing the resistive pulse of a nanoparticle passing through the orifice of a nanopipet. Switching the voltage reverses the direction of the driving force on the particle and allows us to repeatedly pass and measure single nanoparticles. In Figure 1c, the applied voltage and resulting current for two cycles of the particle being passed in and out of the pipet in such a manner are shown. The asymmetry of the resistive pulses seen in conical nanopores is indicative of the direction of travel (negative/left skew implies outward travel), as we have previously reported.[22]

Using programmable data acquisition hardware coupled with voltage switching allows us to dramatically shorten the time taken to switch the force on the particles when compared with traditional data acquisition hardware and our pressure-trapping setup. We demonstrate measurements of single particles at ∼200 times per second, which dramatically shortens
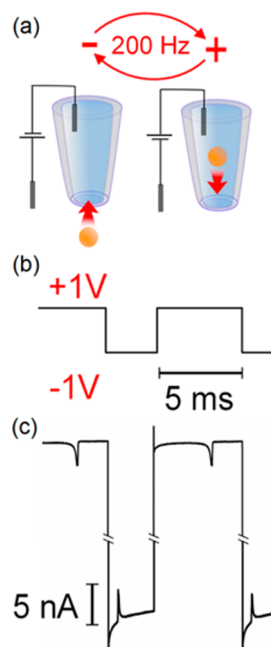
Figure 1. (a) Schematic of experiment measuring individual nanoparticles by passing them back and forth through a nanopipet *via* voltage switching. Short segment of experimentally recorded (b) voltage−time, $V−t$, and (c) current−time, $i−t$, data for four translocations of a single nanoparticle (out−in−out−in sequence). Note the axis break in the i-axis.

the time required to measure the distribution of the resistive pulses from a single particle. This allows us to accurately determine the mean current blockade and deliver improved size resolution. We show that single polystyrene nanoparticles can be trapped and monitored for several minutes, due to the improved switching reducing the chance of losing a trapped particle to essentially nil. This leads to an essentially arbitrary resolution measurement of blockade current, demonstrated by a precisely determined mean blocking current statistically equivalent to resolving particle radii differing by merely 31 pm. While nanoparticles exhibit surface roughness much larger than the demonstrated resolution, the resolution of our volumetric measurements indicates we could differentiate fractional coverage of a monolayer over the entire particle surface. The principle of switching the voltage to measure multiple translocations has previously been reported by Gershow and Golovchenko[37] and Sen and co-workers,[38] who both looked at DNA translocating through symmetric nanochannels/pores.

RESULTS AND DISCUSSION

Figure 2 shows a representative short segment of $i−t$ data resulting from trapping/sizing of a mixture of three nominally 250 nm polystyrene particles. Part a shows three sequential bursts of activity arising from the rapid switching of the voltage and the concomitant rapid changes in the current as three different particles are trapped/sized; individual switching events are not
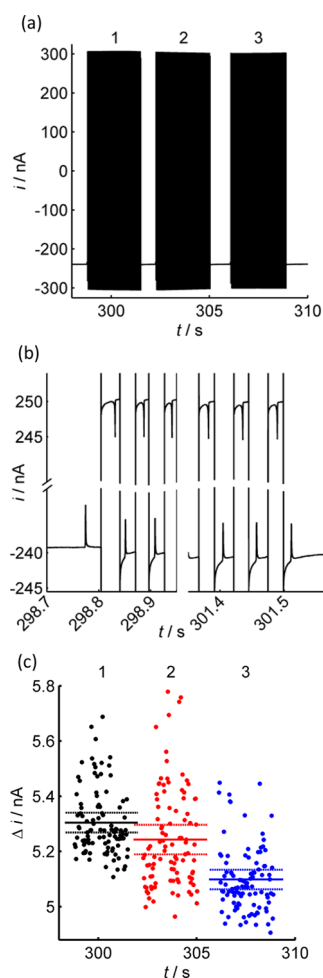
Figure 2. Multipass Coulter counter measurements of three polystyrene particles of 250 nm nominal radius (101 translocations each particle). $i{-}t$ measurements from the trapping of (a) three particles and (b) subsection of the trapping of a single particle (particle 1 in part a) on an expanded current and time range. (c) Amplitude of the current blockade relating to each of the translocations of the three particles shown in part a. Solid horizontal lines represent the mean value of the current blockade for each particle and are flanked by lines at ± 3 standard errors of the mean (SEM) ($\sim$99.7% confidence interval) (0.1 M NaCl with buffer, $\sim$600 nm radius pipet).

resolvable on this scale. In each case the particle enters the pore under the influence of a -1 V potential applied within the pipet, resulting in a $\sim$240 nA current. The particle is passed back and forth through the pipet orifice 100 times, before finally being drawn deep into the pipet, negating the possibility of the same particle being trapped and analyzed a second time. This is visible in Figure 2b, which presents the initial and final portions of the current−time trace for particle 1 and shows resistive pulses, where the current magnitude drops by $\sim$5 nA (2%) as the particle passes through the pipet orifice. After the control software detects a resistive pulse there is a user-defined wait period before the voltage is automatically switched to the opposite polarity (± 1 V in this case); this wait allows for the complete translocation of the particle. The time

between a particle entering (leaving) the pipet and the voltage being switched correlates with the time until the particle is observed leaving (entering) the pipet (see below for more details); however, as the particle is undergoing a (biased) random walk at all times, there is some variability, as we have previously shown.[39]

As the particle enters the pipet under a negative potential, we can assess the magnitude of the competing forces on the particle. At this negative potential, electrophoresis of the negatively charged particle (charge imbued by surface-terminating sulfate groups) acts outward; whereas forces due to the electroosmotically driven fluid flow arising from the negatively charged glass acting inward. As the particle travels inward when a negative potential is applied, we deduce that electroosmotically driven flow is the dominant force for these experimental conditions.

As seen in Figure 2a the time between each burst of activity is variable; this reflects the fact that particles are randomly diffusing in solution and must be close to the pipet orifice before they are influenced by the applied potential/induced fluid flow and can be trapped. The slight difference between the magnitude of the current measured at ± 1 V (-240 *vs* 246 nA) may be down to a slight offset on the amplifier or slight differences in the internal and external concentrations due to evaporation. A charging current occurs after the voltage is switched; this is followed by a slower process that sees the current change by <1 nA over $\sim$10 ms. The direction of this change varies from probe to probe and may be attributable to redistribution of the subtly different ion concentrations inside and outside the pipet. The effect on the measured current blockade is negated by background subtraction, as detailed in the Supporting Information.

The blockades corresponding to the 101 translocations of each particle presented in Figure 2a are presented in Figure 2c. It is immediately apparent that there is considerable spread in the measured blockades for a single particle. This variation, which will be discussed in more detail later, can be attributed to off axial *vs* axial translations and/or asymmetries in the particle.[22,36] The exact distribution of blockades, which in this case show a higher density below the mean, will be a convolution of the likelihood of a particle translating at a particular position/orientation and the blockade for such configuration. The solid horizontal lines represent the mean current blockade for each particle and are flanked by dashed lines that are at ± 3 standard errors of the mean and give a $\sim$99.7% confidence interval of the mean. Comparing the mean and error bounds for particles 2 and 3 demonstrate that they can be confidently distinguished by the voltage-trapping/measuring method. However, it is obvious that the individual measurements from each particle overlap to a large extent, and the particles could not be confidently distinguished based upon any one measurement, as would be performed using a conventional Coulter counter.
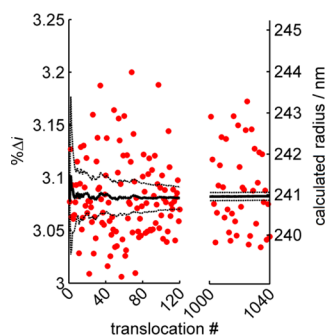
Figure 3. Percentage blockade and computed radius (calculated from eq 1) as a function of translocation number for a single 250 nm nominal radius polystyrene nanoparticle. Red circles represent the blockade percentage for each translocation. The black solid line represents the mean current blockade/mean calculated radius from translocations up to and including the translocation number indicated on the abscissa and is flanked by lines at ±3 SEM (∼99.7% confidence interval). Note the axis break (50 mM NaCl with buffer, ∼500 nm radius pipet).

Figure 3 further demonstrates the benefit of making multiple measurements of an individual particle. The plot shows results from a single particle that underwent over 1000 translocations. The percentage current blockade of each translocation is presented as a red circle, from which we see a variation that ranges over ∼0.2%, a range that equates to more than 4 nm (see below for details of conversion). The solid black line represents the mean blockade up to the translocation number, and the dashed lines represent 3 standard errors of the mean (SEM), which represent a ∼99.7% confidence interval. Initially the confidence interval rapidly decreases with an increasing number of translocations; however, this decay follows a $\sqrt{n}$ relationship, meaning that a 4-fold increase in the number of translocations sees a 2-fold reduction in the error bounds. The resolution can be improved with more translocations, although there is a small cost in terms of an increased duration of the recording. For this system 100 translocations give subnanometer resolution (∼0.6 nm), whereas for 1000 translocations this improves by a factor of $\sqrt{10} \approx 3.2$ to ∼0.2 nm. We have measured single particles for minutes, where >10 000 translocations are observed and the resolution is equivalent to <1 Å (see Supporting Information). The equivalent radius is a statistical measure, which assumes the particle to be perfectly spherical; however, it would allow the resolution of miniscule differences between particles that will have some intrinsic non-ideality (roughness/asphericity).

Figure 4 shows two histogram plots derived from trapping/sizing a sample of 250 nm nominal radius polystyrene particles. Part a shows histograms of percentage current blockade each relating to 101 measurements of eight different *individual* particles. A total of 101 measurements was chosen, as it is sufficient to resolve the particle radius to ∼0.6 nm (see Figure 3).
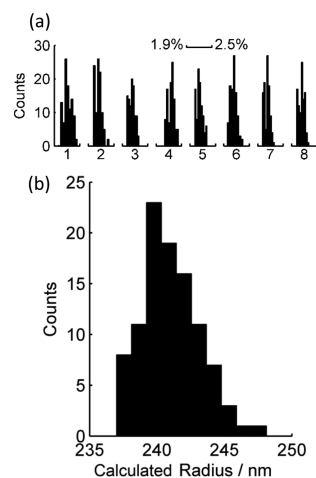
Figure 4. (a) Histograms of the %Δi for eight individual polystyrene particles of 250 nm nominal radius that were each measured 101 times. (b) Histogram of the measured particle size distribution of 100 particles as measured by the multipass Coulter counter. Associated $i-t$ data and 92 additional single-particle histograms are available in the Supporting Information. Note: In part a each "count" refers to one translocation/measurement, whereas in part b "count" refers to one particle (0.1 M NaCl with buffer, ∼600 nm radius pipet).

The variation in the measured blockades is much larger than the instrumentation noise and is largely explained by the variation of the position of the particle as it translocates (axial *vs* off-axis). This variability has been studied theoretically for cylindrical pores, and the ∼15% variability we observe is of comparable size.[28,30,40] These histograms are not accessible to a conventional Coulter counter measurement, where each particle is measured only once. Not only does this allow us to determine the mean blockade current with high precision, but it also allows us to assess the variability of single measurements. Ordinarily the variability would be a combination of variability between particles and variability due to the measurement, whereas through the trapping— measuring we are able to eliminate the former and assess the latter.

The histogram in Figure 4b represents the size distribution of the *population* of 100 particles, each of which was measured 101 times. The percentage blockade histograms of eight are shown in part a (the remaining 92 are available in the Supporting Information). The mean value of each blockade was then converted to a size by[21,23]

$$\%\Delta i = k r^3 \qquad (1)$$

where %Δi is the percentage that the current is blocked at the peak of the translocation, r is the radius of the particle, and k is a constant related to the geometry of the pipet, which is reasonable to use when the electrolyte concentration is high, where electroosmotic and ion current rectification effects are minimal.[41,42] k was determined through defining the population mean to be equal to the mean value measured by scanning electron

microscopy (241 nm, see Supporting Information for details). This value differs from the manufacturer's nominal value (250 nm), but is within their expected tolerances. While a slight discrepancy in this value would shift this distribution slightly, it would not change the resolution or width of any distributions derived to any significant degree. The spread of the distribution measured by voltage trapping (2.3 nm standard deviation) represents an upper limit on the true spread, as some convolution occurs from measurement uncertainty. However, through measuring each particle 101 times, this contribution is small (~0.6 nm). Analysis of scanning electron microscopy images (see Supporting Information) determined the particle size distribution to have a 3 nm standard deviation, which compares favorably with the distribution voltage trapping/measuring. If we consider the inherent spread in resistive pulse amplitudes from individual particles (>4 nm), it would be impossible to resolve such a distribution without a multipass system.

In acquiring the data presented in Figure 4, we never lost a particle due to diffusion; that is, a particle never random walked beyond the region in which we could retrap it until we chose to drive it deep into the pore (after 101 translocations). This reassures us that the possibility of particle switching, *i.e.*, the trapped particle leaving the trapping zone concurrently with a second particle entering, is essentially zero. This is not to say that second particles did not diffuse into the trap; however, in such situations this was immediately apparent as two separate resistive pulses, and those data were not included in the analysis (see Supporting Information for more details). Additionally, some particles were lost due to triggering failures and were also not used in the analysis (see Supporting Information for details).

Figure 5 shows the results from voltage trapping/ measuring of a mixture of polystyrene particles of 250 and 100 nm nominal radii. Each particle was trapped/ measured for 101 translocations before being driven deep into the pipet; the subsequent particle entered from outside the pipet, ensuring that it was a different particle. Figure 5b shows the current time traces from two particles, one with 250 nm nominal radius and one with 100 nm nominal radius, on an expanded current scale. It is immediately apparent that each particle blocks the current by a different amount, as would be expected from eq 1. Nonetheless, we are able to trap and measure both particle sizes with the same pipet and with the same parameters (trigger thresholds, *etc*.).

In Figure 5c the percentage blockade arising from each translocation of the six particles in part a is presented. As is expected, the two populations of particle sizes (250/100 nm nominal radius) are clearly distinguished; moreover, we are able to distinguish the particles within those individual populations. The absolute variability is different between the two populations,
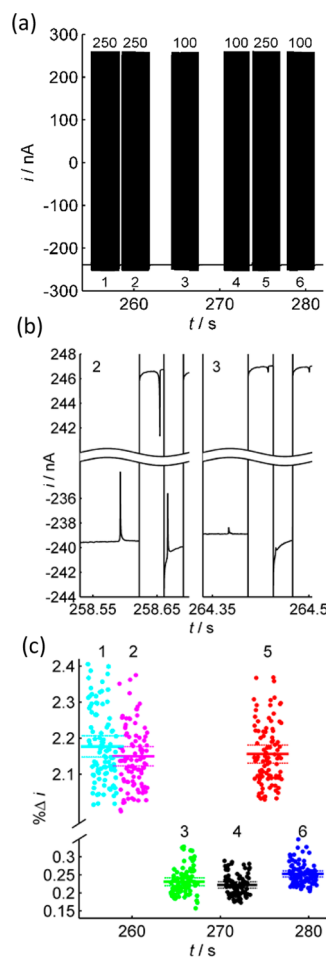
Figure 5. Data for sizing/trapping of six particles from a mixture of 100 and 250 nm nominal radius polystyrene particles. (a) Full-range i−t trace. Each "block" is the current response of a single particle being passed through the pore 101 times by rapidly alternating the applied voltage. Particle nominal sizes are labeled in nm above each trace, and they are numbered below. (b) Initial portion of the i−t traces for particles 2 and 3 with expanded t-axis and a break in the i-axis. Individual particle translocations are now easily resolvable as drops in the current magnitude. (c) %Δi relating to each of the translocations of the particles shown in part a. Solid horizontal lines represent the mean value of the current blockade for each particle and are flanked by lines at ±3 SEM (~99.7% confidence interval) (0.1 M NaCl with buffer, ~600 nm radius pipet). Note the axis break. Expanded traces for all particles are included in the Supporting Information.

with the less blocking, 100 nm nominal radius particles (3, 4, and 6) being spread over a range of 0.15% of the baseline current, whereas the 250 nm nominal radius particles are spread over ~0.4%. However, when we consider the relative variability, it is the smaller particles that show more variability. As the 100 nm particles block only ~0.25% of the current, the peak heights can be affected by instrumentation noise or by any uncertainty in fitting the baseline current.

The radius of each particle was calculated as previously, by setting the mean radius of the larger particles to their value as measured by electron microscopy and then using eq 1. In doing this, the derived radii for the

smaller particles have a mean of ~117 nm, which is close to 108 nm measured by microscopy. This slight difference may be attributable to components of the current that come from electroosmotic flow and which cause a deviation from eq 1. An interpretation of this is that for the conditions in our study k in eq 1 is not constant, but rather is a function that weakly depends on the particle size (~10% change between the two particle sizes).

The software for the trapping/measuring of particles allows the user to decide how long to wait after detecting a translocation before switching the potential; different wait durations can be chosen for translocations at opposite polarities. In Figure 6a a particle enters the pore under a negative potential. When the absolute value of the current gradient (di/dt) is greater than a threshold value, this triggers a timer to initiate; switching occurs when the timer expires (after ~2.5 ms in the schematic). As shown in the figure, we define t_{wait} as the time from the peak of the resistive pulse until the switching time. *NB*: This may differ from the value the user chooses, as triggering can occur part way through a translocation. t_{return} is the time from the potential switching until the particle is redetected. t_{return} depends strongly on t_{wait}, the direction of travel (out of or into the pipet), and the particle size, as shown

(a)

(b)
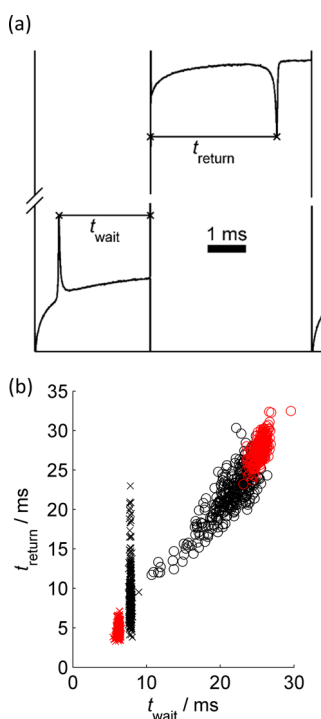
Figure 6. (a) Schematic showing the wait time from the translocation peak until the potential is switched, t_{wait}, and the time until the peak of the next translocation, t_{return}. (b) Plot of t_{return} vs t_{wait} for a mixture of 250 nm (red) and 100 nm (black) nominal radius polystyrene particles. Crosses are from periods where the particle was outside the pipet; circles are from when the particle was inside the pipet (as is shown in part a). This plot contains data from 13 particles, each of which was captured for 101 translocations (0.1 M NaCl with buffer, ~600 nm radius pipet).

in Figure 6b. The crosses at $t_{wait} = 6-7$ ms represent periods when the particle was outside the pipet. We see a spread in the values of t_{return}, which is due to the random walk that particles undertake. The black points represent particles of 100 nm nominal radius; they show a considerably wider distribution than the 250 nm nominal radius particles that are shown in red despite switching occurring at a similar time. We attribute this broadening to the higher diffusion coefficient of the 100 nm nanoparticles. The circles on this plot represent a period when the particle was inside the pipet. Again we notice that for similar values of t_{wait} the variance of the 100 nm (black) particles is greater. However, we notice that even though the particles were inside the pipet for considerably longer, the variation in t_{return} is actually significantly less. The electric field and electroosmotic flow drop off more slowly within the pipet than outside and so can dominate mass transport; furthermore diffusion within the pipet is predominantly one-dimensional, in contrast to three-dimensional diffusion outside. If we consider the black circles, which represent 100 nm particles that have been transported inside the pipet, we observe two things. First, for increasing values of t_{wait} we see increasing values of t_{return} and that the relationship between the two values is approximately linear. This fits intuitively with the idea that the longer the value of t_{wait}, the further the particle is allowed to travel into the pipet before the voltage is switched and thus the further it must travel before exiting the pipet. *NB*: While in this case the gradient is around 1, which is indicative of no pressure-driven flow, pressures within the system can cause it to deviate from this value. Second, one can observe that as t_{wait} increases, there is a broadening in the value of t_{return}. Again, this is in accord with the idea that the particle has more time to diffuse.

Figure 6 reinforces the observation that one is more likely to "lose" a particle when it is outside the pipet than inside (see Supporting Information). It also highlights the importance of rapid switching of the forces (potential) to achieving consistent, stable trapping of particles.

CONCLUSIONS

In this work we demonstrated a high-speed voltage-trapping/measuring Coulter counter that allows us to measure nanoparticles in solution to an essentially arbitrarily high resolution. The resolution demonstrated in this work should be sufficient to resolve the difference in radius from a partial monolayer coverage of a particle. Note that, regardless of the accuracy of the calibration, we expect to resolve a difference in blockade currents. When blockade currents are converted to equivalent radii, errors in calibration will be reflected in errors in the absolute values of radii.

We demonstrated this technique with polystyrene nanoparticles; however, there is no inherent restriction

on the particle material. Electroosmotic flow, which occurs due to the charged groups on the glass wall, will occur and interact with any nanoscopic particulates, regardless of surface charge, conductivity, *etc*. Thus, one could conceivably use it to measure uncharged metallic nanoparticles, nanoscopic biological entities, or even emulsions.[43] For conditions different from those used in this work, such as nonspherical particles,[29] deformable particles,[44] or lower ionic strength solutions,[41,42] current−volume relations different from eq 1 may be necessary. However, the premise of multiple measurements improving resolution and allowing the characterization of variability remains.

In this work we demonstrated trapping of 100 nm particles with angstrom resolution; however, ongoing work in our laboratory, which will be reported in the near future, is demonstrating the extension of this capability to smaller metallic nanoparticles. A good signal-to-noise ratio for resistive pulse measurements can be maintained by shrinking the pipet size (see, for example, ref 34; 4 nm radius particles), where angstrom resolution would represent a larger change in the percentage blockade. However, smaller particles have higher diffusivities, which will likely make them more challenging to trap/measure.

For the system studied in this work there is a limitation on the maximum rate of measuring at around 200 translocations/s (see Supporting Information for an example i−t trace), which already allows for a rapid determination of size distributions. In this work the limit was due to the finite duration of the translocation events, which could easily be shortened through using an amplifier with a higher voltage range that would effect larger forces on the particle.

The samples studied in this work are stable over time; thus we did not observe any changes in the average percentage blockade. However, the ability to trap a particle for minutes delivers the exciting possibility that one could track the change in the size of a particle as a function of time with subsecond time resolution. We anticipate this to be of interest in applications such as nanoparticle synthesis and colloidal formation.

Nanoscale glass or quartz pipets, such as those used in this work, are the scanning probe in the scanning ion conductance microscope (SICM).[45−48] Coupling voltage-trapping/measuring with the distance control capabilities of an SICM would open up the exciting possibility to precisely position a pipet over a characterized area of a surface and to deliver, on command, a characterized nanoparticle or other nanoscopic particulate. A similar concept, but lacking the trapping element, was recently reported by Mirkin and co-workers.[49]

This work has focused on the mean value of the resistive pulse amplitude from which the particle radius can be derived. Previous work using a standard Coulter counter has shown the duration of the translocation to be related to a particle's surface charge. Thus, one should be able to use a voltage-trapping/measuring Coulter counter to discriminate both surface charge and size, which will both benefit from the reduced uncertainty from repeated measurements. While this work used eq 1 to relate the blockage current to radius, and in doing so implicitly assumed a spherical particle, Coulter counters are sensitive to the orientation of nonspherical particles.[29] We anticipate that the multipass Coulter counter should be sensitive to this either through larger variation in the peak blockage current or through resolving the tumbling of particles in each pass.

The pore in this work is at the end of a glass pipet; however, electroosmotic flow is a phenomenon that also occurs in channels of micro-nanofluidic devices. Thus, it should be possible to implement the strategy presented in this work as part of such a device, with the possibilities of parallelization and batch production being just some of the possible benefits.

METHODS

Particle sizing measurements were performed in a solution of 50 or 100 mM NaCl (Fisher) with 10 mM PBS and 0.1 vol % Triton X100 in ultrapure water (Barnstead Smart2Pure, Thermo Scientific); the NaCl concentration for each measurement is reported with the data. The solution was adjusted to pH 7.2 with NaOH and filtered through a 0.1 μm filter (Durapore PVDF, Millex) prior to use. Particles were purchased from Polybead microspheres (Polyscience) and were sonicated and added to the external solution to give concentrations of 5×10^7 to 2×10^9 particles/mL. Measurements were performed in a ~1 mL volume in an Eppendorf tube.

Pipets were prepared by pulling 1.0 mm outer diameter 0.7 mm inner diameter quartz capillaries (Q100-70-7.5, Sutter) in a P-2000 laser puller (Sutter). The capillaries were first washed inside and out with ultrapure water and dried with N_2. A single line program was used with the following parameters: heat 439−465, filament 1, velocity 30, delay 145, pull 175, where the heat parameter was chosen to give a suitable pipet size. Pipets were backfilled using a Microfil (MF28G, World Precision Instruments). A small air bubble that remained trapped at the tip of the pipet was pushed out by back-connecting the pipet to a N_2 cylinder and slowly ramping the pressure while the tip of the pipet remained in water. The pressure at which the air bubble exited the pipet was used to size the pipet as described in ref 50. The filled pipet was mounted in a pipet holder (MEW-M10FL, Warner) containing a Ag/AgCl wire. A Ag/AgCl wire was also used as the external electrode.

All particle trapping experiments were performed inside a Faraday cage. The voltage was applied and current recorded by a patch clamp amplifier (Heka, EPC10 USB), which was connected to field programmable gate array data acquisition card (FPGA card, PCIe-7852R, National Instruments) through the analog channels of both components. Details on the filter/gain settings, which were chosen to avoid distorting peak shapes/digitization, are available in the Supporting Information.

The program running on the FPGA card, written using the LabVIEW FPGA module, continually calculated the derivative of the current (calculated from a least-squares fit) and instigated a voltage switching protocol when the magnitude was above a user-defined threshold level. Data were passed to a LabVIEW

program running on the computer that presented the data to the user in real time and which communicated with the FPGA card to update the settings of the voltage switching protocol. More details of the software and switching protocol are available in the discussion of Figure 2, and a discussion of triggering is included in the Supporting Information. The data acquisition/transfer part of the software was based, in part, on similar functions in the Warwick Electrochemical Scanning Probe Microscopy software suite[51] (University of Warwick).

REFERENCES AND NOTES

1. Daniel, M.-C.; Astruc, D. Gold Nanoparticles: Assembly, Supramolecular Chemistry, Quantum-Size-Related Properties, and Applications toward Biology, Catalysis, and Nanotechnology. *Chem. Rev.* **2004**, *104*, 293–346.

2. Kleijn, S. E. F.; Lai, S. C. S.; Koper, M. T. M.; Unwin, P. R. Electrochemistry of Nanoparticles. *Angew. Chem., Int. Ed.* **2014**, *53*, 3558–3586.

3. Murray, R. W. Nanoelectrochemistry: Metal Nanoparticles, Nanoelectrodes, and Nanopores. *Chem. Rev.* **2008**, *108*, 2688–2720.

4. Na, H. B.; Song, I. C.; Hyeon, T. Inorganic Nanoparticles for MRI Contrast Agents. *Adv. Mater.* **2009**, *21*, 2133–2148.

5. Tromsdorf, U. I.; Bigall, N. C.; Kaul, M. G.; Bruns, O. T.; Nikolic, M. S.; Mollwitz, B.; Sperling, R. A.; Reimer, R.; Hohenberg, H.; Parak, W. J.; et al. Size and Surface Effects on the MRI Relaxivity of Manganese Ferrite Nanoparticle Contrast Agents. *Nano Lett.* **2007**, *7*, 2422–2427.

6. Alivisatos, A. P. Semiconductor Clusters, Nanocrystals, and Quantum Dots. *Science* **1996**, *271*, 933–937.

7. Dick, J. E.; Hilterbrand, A. T.; Boika, A.; Upton, J. W.; Bard, A. J. Electrochemical Detection of a Single Cytomegalovirus at an Ultramicroelectrode and Its Antibody Anchoring. *Proc. Natl. Acad. Sci. U. S. A.* **2015**, *112*, 5303–5308.

8. Li, Y.-T.; Zhang, S.-H.; Wang, L.; Xiao, R.-R.; Liu, W.; Zhang, X.-W.; Zhou, Z.; Amatore, C.; Huang, W.-H. Nanoelectrode for Amperometric Monitoring of Individual Vesicular Exocytosis Inside Single Synapses. *Angew. Chem., Int. Ed.* **2014**, *53*, 12456–12460.

9. Dunevall, J.; Fathali, H.; Najafinobar, N.; Lovric, J.; Wigström, J.; Cans, A.-S.; Ewing, A. G. Characterizing the Catecholamine Content of Single Mammalian Vesicles by Collision–Adsorption Events at an Electrode. *J. Am. Chem. Soc.* **2015**, *137*, 4344–4346.

10. Dick, J. E.; Renault, C.; Bard, A. J. Observation of Single-Protein and DNA Macromolecule Collisions on Ultramicroelectrodes. *J. Am. Chem. Soc.* **2015**, *137*, 8376–8379.

11. http://www.sigmaaldrich.com/catalog/product/fluka/95585?lang=en&region=US accessed on August 22, 2015.

12. Brar, S. K.; Verma, M. Measurement of Nanoparticles by Light-Scattering Techniques. *TrAC, Trends Anal. Chem.* **2011**, *30*, 4–17.

13. De Vos, C.; Deriemaeker, L.; Finsy, R. Quantitative Assessment of the Conditioning of the Inversion of Quasi-Elastic and Static Light Scattering Data for Particle Size Distributions. *Langmuir* **1996**, *12*, 2630–2636.

14. Azubel, M.; Koivisto, J.; Malola, S.; Bushnell, D.; Hura, G. L.; Koh, A. L.; Tsunoyama, H.; Tsukuda, T.; Pettersson, M.; Hakkinen, H.; et al. Electron Microscopy of Gold Nanoparticles at Atomic Resolution. *Science* **2014**, *345*, 909–912.

15. Park, J.; Elmlund, H.; Ercius, P.; Yuk, J. M.; Limmer, D. T.; Chen, Q.; Kim, K.; Han, S. H.; Weitz, D. A.; Zettl, A.; et al. 3D Structure of Individual Nanocrystals in Solution by Electron Microscopy. *Science* **2015**, *349*, 290–295.

16. Domingos, R. F.; Baalousha, M. A.; Ju-Nam, Y.; Reid, M. M.; Tufenkji, N.; Lead, J. R.; Leppard, G. G.; Wilkinson, K. J. Characterizing Manufactured Nanoparticles in the Environment: Multimethod Determination of Particle Sizes. *Environ. Sci. Technol.* **2009**, *43*, 7277–7284.

17. Talmon, Y. Staining and Drying-Induced Artifacts in Electron Microcsopy of Surfactant Dispersions. *J. Colloid Interface Sci.* **1983**, *93*, 366–382.

18. Filipe, V.; Hawe, A.; Jiskoot, W. Critical Evaluation of Nanoparticle Tracking Analysis (NTA) by NanoSight for the Measurement of Nanoparticles and Protein Aggregates. *Pharm. Res.* **2010**, *27*, 796–810.

19. Coulter, W. H. Means for Counting Particles Suspended in a Fluid. U.S. Patent 2656508, October 20, 1953.

20. DeBlois, R. W.; Bean, C. P. Counting and Sizing of Submicron Particles by the Resistive Pulse Technique. *Rev. Sci. Instrum.* **1970**, *41*, 909–916.

21. Ito, T.; Sun, L.; Crooks, R. M. Simultaneous Determination of the Size and Surface Charge of Individual Nanoparticles Using a Carbon Nanotube-Based Coulter Counter. *Anal. Chem.* **2003**, *75*, 2399–2406.

22. Lan, W.-J.; Holden, D. A.; Zhang, B.; White, H. S. Nanoparticle Transport in Conical-Shaped Nanopores. *Anal. Chem.* **2011**, *83*, 3840–3847.

23. Vogel, R.; Willmott, G.; Kozak, D.; Roberts, G. S.; Anderson, W.; Groenewegen, L.; Glossop, B.; Barnett, A.; Turner, A.; Trau, M. Quantitative Sizing of Nano/microparticles with a Tunable Elastomeric Pore Sensor. *Anal. Chem.* **2011**, *83*, 3499–3506.

24. Harms, Z. D.; Mogensen, K. B.; Nunes, P. S.; Zhou, K.; Hildenbrand, B. W.; Mitra, I.; Tan, Z.; Zlotnick, A.; Kutter, J. P.; Jacobson, S. C. Nanofluidic Devices with Two Pores in Series for Resistive-Pulse Sensing of Single Virus Capsids. *Anal. Chem.* **2011**, *83*, 9573–9578.

25. DeBlois, R. W.; Bean, C. P.; Wesley, R. K. A. Electrokinetic Measurements with Submicron Particles and Pores by the Resistive Pulse Technique. *J. Colloid Interface Sci.* **1977**, *61*, 323–335.

26. Kozak, D.; Anderson, W.; Vogel, R.; Chen, S.; Antaw, F.; Trau, M. Simultaneous Size and ζ-Potential Measurements of Individual Nanoparticles in Dispersion Using Size-Tunable Pore Sensors. *ACS Nano* **2012**, *6*, 6990–6997.

27. Berge, L. I. Single Particle Flow Dynamics in Small Pores by the Resistive Pulse and the Pressure Reversal Technique. *J. Colloid Interface Sci.* **1990**, *138*, 480–488.

28. Qiu, Y.; Hinkle, P.; Yang, C.; Bakker, H. E.; Schiel, M.; Wang, H.; Melnikov, D.; Gracheva, M.; Toimil-Molares, M. E.; Imhof, A.; et al. Pores with Longitudinal Irregularities Distinguish Objects by Shape. *ACS Nano* **2015**, *9*, 4390–4397.

29. Qin, Z.; Zhe, J.; Wang, G.-X. Effects of Particle's Off-Axis Position, Shape, Orientation and Entry Position on Resistance Changes of Micro Coulter Counting Devices. *Meas. Sci. Technol.* **2011**, *22*, 045804.

30. Golibersuch, D. C. Observation of Aspherical Particle Rotation in Poiseuille Flow *via* the Resistance Pulse Technique. *Biophys. J.* **1973**, *13*, 265–280.

31. Holden, D. A.; Watkins, J. J.; White, H. S. Resistive-Pulse Detection of Multilamellar Liposomes. *Langmuir* **2012**, *28*, 7572–7577.

32. Pevarnik, M.; Schiel, M.; Yoshimatsu, K.; Vlassiouk, I. V.; Kwon, J. S.; Shea, K. J.; Siwy, Z. S. Particle Deformation and Concentration Polarization in Electroosmotic Transport of Hydrogels through Pores. *ACS Nano* **2013**, *7*, 3720–3728.

33. Holden, D. A.; Hendrickson, G. R.; Lan, W.-J.; Lyon, L. A.; White, H. S. Electrical Signature of the Deformation and Dehydration of Microgels during Translocation through Nanopores. *Soft Matter* **2011**, *7*, 8035–8040.

34. German, S. R.; Luo, L.; White, H. S.; Mega, T. L. Controlling Nanoparticle Dynamics in Conical Nanopores. *J. Phys. Chem. C* **2013**, *117*, 703–711.

35. German, S. R.; Hurd, T. S.; White, H. S.; Mega, T. L. Sizing Individual Au Nanoparticles in Solution with Sub-Nanometer Resolution. *ACS Nano* **2015**, *9*, 7186–7194.

36. Berge, L. I.; Jossang, T.; Feder, J. Off-Axis Response for Particles Passing through Long Apertures in Coulter-Type Counters. *Meas. Sci. Technol.* **1990**, *1*, 471–474.

37. Gershow, M.; Golovchenko, J. A. Recapturing and Trapping Single Molecules with a Solid-State Nanopore. *Nat. Nanotechnol.* **2007**, *2*, 775–779.

38. Sen, Y.-H.; Jain, T.; Aguilar, C. A.; Karnik, R. Enhanced Discrimination of DNA Molecules in Nanofluidic Channels through Multiple Measurements. *Lab Chip* **2012**, *12*, 1094–1101.

39. Lan, W.-J. J.; White, H. S. Diffusional Motion of a Particle Translocating through a Nanopore. *ACS Nano* **2012**, *6*, 1757–1765.

40. Stober, G.; Steinbock, L. J.; Keyser, U. F. Modeling of Colloidal Transport in Capillaries. *J. Appl. Phys.* **2009**, *105*, 084702.

41. Lan, W.-J.; Kubeil, C.; Xiong, J.-W.; Bund, A.; White, H. S. Effect of Surface Charge on the Resistive Pulse Waveshape during Particle Translocation through Glass Nanopores. *J. Phys. Chem. C* **2014**, *118*, 2726–2734.

42. Steinbock, L. J.; Stober, G.; Keyser, U. F. Sensing DNA-Coatings of Microparticles Using Micropipettes. *Biosens. Bioelectron.* **2009**, *24*, 2423–2427.

43. Kim, B.-K.; Boika, A.; Kim, J.; Dick, J. E.; Bard, A. J. Characterizing Emulsions by Observation of Single Droplet Collisions—Attoliter Electrochemical Reactors. *J. Am. Chem. Soc.* **2014**, *136*, 4849–4852.

44. Holden, D. A.; Hendrickson, G. R.; Lan, W.-J.; Lyon, L. A.; White, H. S. Electrical Signature of the Deformation and Dehydration of Microgels during Translocation through Nanopores. *Soft Matter* **2011**, *7*, 8035–8040.

45. Edwards, M. A.; Williams, C. G.; Whitworth, A. L.; Unwin, P. R. Scanning Ion Conductance Microscopy: A Model for Experimentally Realistic Conditions and Image Interpretation. *Anal. Chem.* **2009**, *81*, 4482–4492.

46. Hansma, P. K.; Drake, B.; Marti, O.; Gould, S. A.; Prater, S. A. The Scanning Ion Conductance Microscope. *Science* **1989**, *243*, 641–643.

47. Chen, C.-C.; Zhou, Y.; Baker, L. A. Scanning Ion Conductance Microscopy. *Annu. Rev. Anal. Chem.* **2012**, *5*, 207–228.

48. Korchev, Y. E.; Bashford, C. L.; Milovanovic, M.; Vodyanoy, I.; Lab, M. J. Scanning Ion Conductance Microscopy of Living Cells. *Biophys. J.* **1997**, *73*, 653–658.

49. Wang, Y.; Cai, H.; Mirkin, M. V. Delivery of Single Nanoparticles from Nanopipettes under Resistive-Pulse Control. *ChemElectroChem* **2015**, *2*, 343–347.

50. Mittman, S.; Flaming, D. G.; Copenhagen, D. R.; Belgum, J. H. Bubble Pressure Measurement of Micropipet Tip Outer Diameter. *J. Neurosci. Methods* **1987**, *22*, 161–166.

51. Nadappuram, B. P.; McKelvey, K. M.; Al-Botros, R.; Colburn, A. W.; Unwin, P. R. Fabrication and Characterization of Dual Function Nanoscale pH-Scanning Ion Conductance Microscopy (SICM) Probes for High Resolution pH Mapping. *Anal. Chem.* **2013**, *85*, 8070–8074.